π-Conjugated Materials as the Hole-Transporting Layer in Perovskite Solar Cells

Alexandre Gheno, Sylvain Vedraine, Bernard Ratier, Johann Bouclé

metals

MDPI

Review

π-Conjugated Materials as the Hole-Transporting Layer in Perovskite Solar Cells

Alexandre Gheno, Sylvain Vedraine, Bernard Ratier and Johann Bouclé *

Received: 4 December 2015; Accepted: 5 January 2016; Published: 12 January 2016
Academic Editor: Bruno Schmaltz

XLIM UMR 7252, Université de Limoges/CNRS, Faculté des Sciences et Techniques de Limoges, 87060 Limoges Cedex, France; alexandre.gheno@etu.unilim.fr (A.G.); sylvain.vedraine@unilim.fr (S.V.); bernard.ratier@unilim.fr (B.R.)
* Correspondence: johann.boucle@unilim.fr; Tel.: +33-5-87-50-67-62; Fax: +33-5-55-45-76-49

Abstract: Hybrid organometal halide perovskites have attracted much attention these past four years as the new active layer for photovoltaic applications. Researches are now intensively focused on the stability issues of these solar cells, the process of fabrication and the design of innovative materials to produce efficient perovskite devices. In this review, we highlight the recent progress demonstrated in 2015 in the design of new π-conjugated organic materials used as hole transporters in such solar cells. Indeed, several of these "synthetic metals" have been proposed to play this role during the last few years, in an attempt to replace the conventional 2,2′,7,7′-tetrakis-(*N*,*N*-di-4-methoxyphenylamino)-9,9′-spirobifluorene (Spiro-OMeTAD) reference. Organic compounds have the benefits of low production costs and the abundance of raw materials, but they are also crucial components in order to address some of the stability issues usually encountered by this type of technology. We especially point out the main design rules to reach high efficiencies.

Keywords: perovskite; solar cells; HTM; hole transport materials; molecular glasses; synthetic metals

1. Introduction to Hybrid Organometal Halide Perovskite Materials

Within the last five years, a new class of photovoltaic materials made an impressive arrival in the field of solar energy conversion: the organic-inorganic halide perovskites, or hybrid perovskites. In general, the term perovskite defines a kind of crystalline structure composed of three different species (A, B and X) forming the general ABX_3 formula. A and B are two cations of very different sizes and X an anion. In the ideal perovskite structure, the big A^+ cations are at the corners of a cube; the anions X^- are in the middle of each faces; and the small B^{2+} cations are in the middle of the octahedral sites formed by the anions X^- (Figure 1) [1,2].

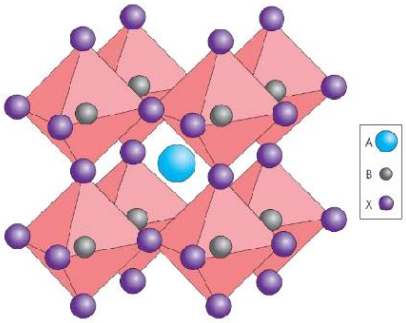

Figure 1. Generic perovskite structure. Reprinted by permission from Macmillan Publishers Ltd: Nature Photonics [2], Copyright 2014.

In hybrid perovskites, the X anion is in fact a halide: an atom of fluorine, chlorine (Cl), bromine or iodine (I). The halide anions' site can also be used by a mixture of different halide atoms, leading to mixed halide perovskites. The small B cations are usually lead (Pb); tin (Sn) can also be used, but the resulting material is found to be less stable, as it can form SnI_4 inside the perovskite phase [2]. These anions and little cations form the inorganic part of the hybrid perovskites. The organic part corresponds to the big cation A: an organic molecule, such as methylammonium ($CH_3NH_3^+$), is commonly used and is sometimes replaced by ethylammonium ($CH_3CH_2NH_3^+$) or formamidinium ($NH_2CH{=}NH_2^+$). Finally, for the photovoltaic application, the most investigated hybrid perovskites are $CH_3NH_3PbI_3$ or the mixed-halide compound $CH_3NH_3PbI_{3-x}Cl_x$.

Hybrid perovskite shows some interesting physical properties to be the source of this outstanding photovoltaic ability. First of all, at room temperature, the material exhibits an averaged disordered cubic phase (space group *Pm*3*m*). This distortion is due to the ammonium rotation and the lead halide octahedral tilt. Such a structure leads to a direct band-gap structure. Furthermore, a spin-orbit coupling lowers the band-gap value by more than 0.8 eV [3]. Halide perovskites are also characterized by a high carrier diffusion length for about one micron, effective mobilities of roughly 10 $cm^2 \cdot V^{-1} \cdot s^{-1}$ and exciton binding energy of ~40 meV [4].

Despite the fact that the photovoltaic behavior of perovskites was known since 1956 [5], we had to wait until 2006 to see the first direct application of a hybrid perovskite as the active layer of a solar cell. Hybrid perovskite was then used as the photo-sensitizer in liquid dye-sensitized solar cells demonstrating 2.2% efficient devices under full sun illumination condition in 2006 [6], before achieving 3.8% in 2009 [7]. However, the solar cells' performances were highly unstable and deteriorated within a few minutes. The real breakthrough occurred in 2012 with two publications reporting efficiencies up to 10% [8,9], representing the first uses of the perovskite as sensitizers of the mesostructured TiO_2 in solid-state devices. Since these reports, much progress has been made in the composition, fabrication and post-processing of the different layers that compose these perovskite solar cells. Today, certified state-of-the-art performances are reported at 20.1% by the Korean Research Institute of Chemical Technology (KRICT), and several groups demonstrated efficiencies over 19% [10], illustrating the strong potentialities of perovskite materials among thin film technologies.

2. Perovskite Solar Cells

Perovskite solar cells first appeared using a direct device architecture, similar to that of the solid state dye-sensitized cell (ssDSSC). This common device architecture is composed of six layers (Figure 2), which allow several combinations of materials. Here, we describe the most common association.

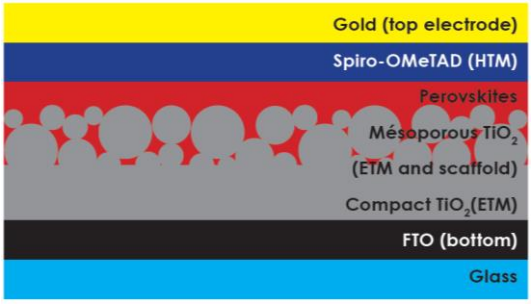

Figure 2. Direct perovskite solar cell architecture. Spiro-OMeTAD, 2,2′,7,7′-tetrakis-(*N*,*N*-di-4-methoxyphenylamino)-9,9′-spirobifluorene; FTO, fluorine-doped tin oxide.

The transparent electrode, made from fluorine-doped tin oxide (FTO), is coated with an electron transporting layer (ETL) mode of compact TiO_2. In some cases, an additional mesoporous TiO_2 layer in used on top of the ETL. This porous electrode is not mandatory. Although this choice is associated with slightly different device behavior, both possibilities can achieve highly efficient devices. If present, the

mesoporous TiO_2 acts as a scaffold for the photo-active perovskite layer, which is deposited (usually from solution) on top of it. Without the porous metal oxide, a quite flat multi-layer architecture is achieved after the deposition of the perovskite absorber.

A hole transport layer (HTL) is deposited on top of the perovskite, followed by the evaporation of a metallic top electrode, usually made of a high work function metal, such as gold. As well as in ssDSSC, the reference HTL material is the organic 2,2′,7,7′-tetrakis-(*N*,*N*-di-4-methoxyphenylamino)-9,9′-spirobifluorene (Spiro-OMeTAD) molecular glass, although intense research efforts are currently being conducted to find relevant alternatives. We give an overview of such recent strategies in the next sections of this article.

The operating principle of the cell is depicted in Figure 3. Incident photons reach the perovskite layer through the transparent electrode, leading to the formation of excitons, which are found to be easily dissociated into free charge carriers in ambient conditions. As mentioned in the previous section, the exciton binding energy is dependent on the composition of the perovskite, as well as the optical gap. In any case, free charge carriers are efficiently created and transported to the ETL and HTL interfaces due to high diffusion length for both electrons and holes [4]. The HTL and ETL ensure selective charge collection at the electrode, while reducing recombination events.

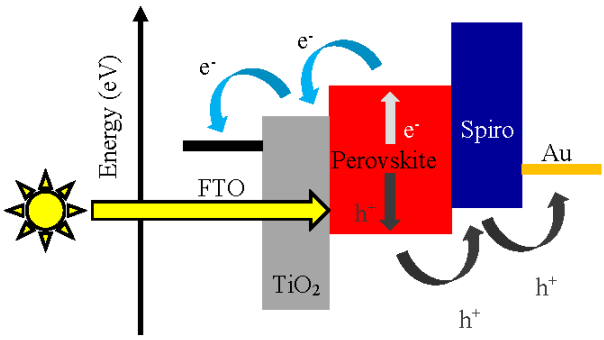

Figure 3. Operating principle scheme of a perovskite solar cell in a direct device architecture (electrons are collected by the transparent FTO electrode).

Apart from the direct device architecture described above, where electrons are collected by the transparent electrode (FTO), the use of various ETL and HTL materials enabled the demonstration of an efficient inverted device architecture, where holes are collected through the transparent electrodes. Such an evolution has the benefit of the possibility to explore low temperature interfacial materials, leading to flexible devices deposited on plastic substrates, for example. In general, an inverted architecture is composed of an HTL deposited on the transparent electrode. The reference HTL material is generally poly(3,4-ethylenedioxythiophene) doped with poly(styrenesulfonate) (PEDOT:PSS), a *p*-type conducting polymer largely exploited in the field of organic solar cells. Other choices of materials will be reviewed in the next sections of this paper. The perovskite absorber is deposited from solution on top of the HTL, before subsequent deposition of the ETL, usually a fullerene derivative, such as phenyl-C61-butyric acid methyl ester (PC61BM). A silver or aluminum top electrode completes the device.

3. Characteristics of Hole Transporting Material for Perovskite Solar Cells

In this section, we present the different features that HTL materials must exhibit for efficient perovskite solar cells. Several reviews addressing the main features of perovskite solar cells, including HTL materials, have been recently published [1,2,11–13]. In this work, we especially focus on the recent developments made both for direct and inverted device architectures. As explained in the first part, the most commonly-used perovskites for efficient devices are today $CH_3NH_3PbI_3$ and $CH_3NH_3PbI_{3-x}Cl_x$. These two kinds of perovskites are in fact very comparable. The most important thing for the hole

transporting material (HTM) is to facilitate hole transfer processes from the perovskite layer, by presenting suitable energy levels adapted to the band gap of the used perovskite, as schematically presented in the Figure 4. The HTM should therefore present the highest occupied molecular orbital (HOMO) energy slightly superior to that of the perovskites, in order to provide the suitable driving force for charge transfer. Furthermore, its lowest unoccupied molecular orbital LUMO level should be significantly lower than that of the perovskites absorbers. This implies that, for example, some HTM will be more suitable for $CH_3NH_3PbI_3$ than for $CH_3NH_3PbI_{3-x}Cl_x$.

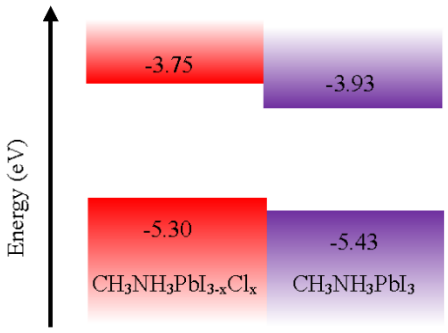

Figure 4. Flat band energy levels of the most commonly-used perovskite absorbers.

Moreover, some HTM materials lead to better photovoltaic performances depending on the chosen device architecture (direct or inverted) and the fabrication process. For direct configurations processed from solution using techniques, such as spray-coating, spin-coating or printing, the best HTM are those that do not require strong polar and protic solvent, as such solvents could dissolve the perovskite layer. However, the HTM solvent should exhibit a good affinity with the surface of the perovskites. To get a better understanding of perovskite layer surface energy and its impact on solution-processing of the solar cell, we performed surface energy measurements with various solvents on $CH_3NH_3PbI_{3-x}Cl_x$ (Table 1).

Table 1. Contact angles measured for 3 solvents (water, ethylene glycol and ethanol) on a $CH_3NH_3PbI_{3-x}Cl_x$ layer and the surface energy of perovskites $CH_3NH_3PbI_{3-x}Cl_x$.

Contact Angles Measurements with Sessile Drop Technique	
Liquid	Contact angle
Water	49.8°
Ethylene glycol	26.6°
Ethanol	7.3°
Surface Energy (Owens–Wendt Theory) (mJ· m^{-2})	
γ_S (γ_d + γ_p)	51.92
γ_d	6.18
γ_p	45.74

These measurements have been made on 600 nm-thick $CH_3NH_3PbI_{3-x}Cl_x$ layers, spin coated directly on glass and annealed in air at 90 °C during 120 min. In the Owens-Wendt theory, the total surface energy of a material (γ_S) is the sum of two values: the value of the polar contribution (γ_p), which accounts for the polarity of the molecules of the material, and the value of the dispersive contribution (γ_d), which accounts for the van der Waals interaction (among other adhesion causes). Note that surface energy measurements are dependent on several factors, like adsorption of water at the tested surface. Furthermore, Owens-Wendt theory does not take into account the surface roughness, which however plays an important role in the spreading of liquid. In any case, these results show that the surface energy of the perovskite layer is primarily (for about 88%) due to polar interactions.

This result shows that, in principle, the solvent of the HTM should have a surface tension energy with a high polar contribution in order to tie in with the polar-oriented profile of the perovskite surface energy. The surface tension of a liquid is defined by its main solvent, but also by the species in suspension or in dilution: in other words, the presence of an HTM can completely modify the surface tension profile of the solvent. Perovskites are also sensitive to humidity, possibly oxygen and doping from other layers: a perfect HTL would be a layer that protects perovskite material from the air and prevents the diffusion of external moieties or elements inside the absorber. Moreover, a perfect HTM would have to properly fill the porosity of the scaffold mesoporous layer (when used). Finally, as the HTM is deposited second to last in the inverted architecture, it should be associated with a low annealing temperature and a short annealing time in order to avoid any degradation of the underlying materials. Typically, the suitable post-processing upper limit is to use an annealing temperature of 70 °C, for around 30 min.

The material requirements are quite different for the inverted device architecture, where hole collection occurs in the transparent electrode. In this case, the perovskite layer is deposited on top of the HTL, and so, its wettability for the perovskite precursor solution has to be suitable for the good spreading of the solution. The HTL should also resist the solvent of the perovskite solution, typically dimethyl sulfoxide (DMSO), isopropanol, *N*–*N* dimethylformamide (DMF) or gamma-butyrolactone (GBL). As an example, we measured the surface tension of a perovskite solution composed of 59 wt. % of DMF, 40 wt. % of perovskite ($PbCl_2$ and CH_3NH_3I with a 1:3 molar ratio) and 1 wt. % of diiodooctane. The surface tension is found to be 39.03 $mN \cdot m^{-1}$ as measured with the pendant drop technique, at a temperature of 20.8 °C in ambient atmosphere. This value is pretty close to the surface tension value of pristine DMF at the same temperature (36.7 $mN \cdot m^{-1}$).

Apart from its rheological behavior, any HTL should also exhibit an optical transmission spectrum compatible with the absorption of the perovskite layer: the transmission of the HTL should be maximal at the maximum of the perovskite absorption, so that most of the incident photons can be absorbed in the photo-active absorber. Figure 5 represents the transmittance of a $CH_3NH_3PbI_{3-x}Cl_x$ film spin coated on a glass substrate and helps to visualize which wavelengths are the most absorbed by the perovskite (and the glass). Any significant absorption of the HTL within the 400–750-nm range would lead to a reduction of the photo-generated current. At last, the HTL must show suitable thermal properties to resist to the annealing treatment of the perovskite layer (in the case of inverted architectures), usually performed at 110 °C for 120 min.

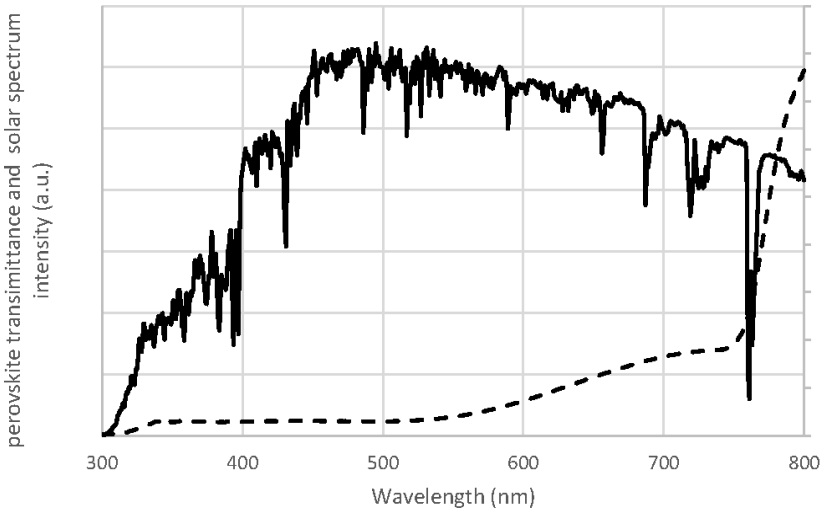

Figure 5. Transmittance of the $CH_3NH_3PbI_{3-x}Cl_x$ perovskite on glass substrate (dotted line, XLIM Research Institute) and the standard AM1.5G solar spectrum (continuous line, IEC 60904-3 Edition 2 (2008)).

4. Classical Pi-Conjugated Materials for Hole Transport

4.1. PEDOT:PSS

PEDOT:PSS (Figure 6) is the most commonly-used HTM for perovskite solar cells in the inverted architecture. Its first use was demonstrated in 2013 [11], the objective being to build a planar heterojunction with $CH_3NH_3PbI_3$ as the donor of electrons and $PC_{61}BM$ as the electron acceptor. Such a configuration reached a power conversion efficiency of 3.9%. Another study a few month later in 2013 was able to largely improve this first value up to 7.9% using the same architecture [14]. PEDOT:PSS is much appreciated, as it allows the production of flexible solar cells. Furthermore, it was the first HTL to allow the use of low temperature processes (<130 °C). In this context, and after several improvement of the perovskite layer, either using the physical deposition method (sublimation under high vacuum) or solution processing, the efficiency of planar perovskite devices was further improved up to 12% using PEDOT:PSS [15,16]. In 2015, using an original strategy for the perovskite film formation, a similar device architecture was reported with an efficiency of 18.1% associated with a 0.16-cm^2 active area, while a photovoltaic module composed of 10 subcells of 4 cm^2 reached 12.9% efficiency (with an open-circuit voltage of 10.1 V, a short-circuit density of 80 mA and a fill factor of 63.7%) [17]. PEDOT:PSS has the advantage of being a very well-known, affordable and easily-available copolymer, extensively investigated in the field of organic solar cells. Its main drawbacks are: (i) its acidity, which is a problem for some transparent conductive layer (such as ITO); and (ii) its high conductivity (~1 $S \cdot cm^{-1}$), which makes it difficult to define the exact active area of the device at the laboratory scale. Underestimation of the area of the cells leads to an overestimation of the efficiency.

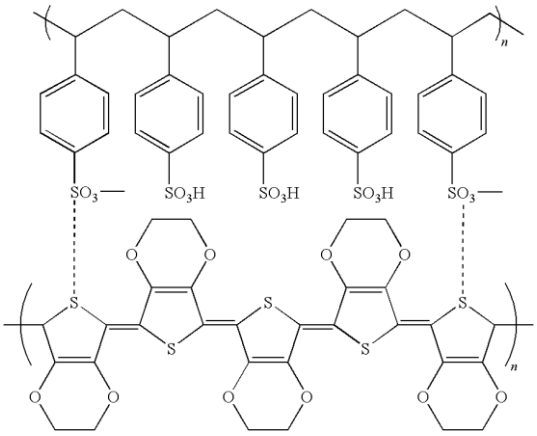

Figure 6. Chemical structure of PEDOT:PSS.

4.2. Spiro-OMeTAD

The first solid-state HTM used with perovskite-sensitized TiO_2 electrodes was the well-known Spiro-OMeTAD. This organic molecular glass was preliminary used in the solid state dye-sensitized solar cell (ssDSSC) architecture (Figure 2) due to its ability to infiltrate at high concentrations the nanoscale porosity of monocrystalline TiO_2 electrodes over several microns thick. Both Grätzel and Snaith's groups were the first to report in 2012 its association with hybrid perovskite absorbers [8,9]. At that time, the best device efficiency was 10% with a short-circuit current-density (J_{SC}) of 17.6 $mA \cdot cm^{-2}$ and an open-circuit voltage (V_{OC}) of 888 mV, showing the strong potentialities of perovskite devices.

In 2014, and after various optimization of the active layer properties and processing steps, the state-of-the-art certified-power conversion efficiency reached 19.3% under full sun in planar cell geometry (ssDSSC architecture without the mesoporous TiO2 scaffold) that incorporates

Spiro-OMeTAD [10]. This cell demonstrated a fill factor of 75%, a J_{SC} of 22.75 mA·cm^{-2} and a V_{OC} of 1.13 V.

The main advantage of Spiro-OMeTAD (Figure 7) is that it possesses a large solubility and a reasonably large hole mobility, and it does not required any post-annealing step. Its suitable affinity with the perovskite layer, associated with a favorable energetic configuration, also reduces charge recombination, leading to a reduction of the potential losses. Spiro-OMeTAD remains the most efficient HTM up to now. Its main drawbacks are the requirement for doping strategies, in order to improve its intrinsic charge mobility. This doping, based on the use of various chemicals (tri-*tert*-butylpyridine (tBp), lithium bis-trifluoromethanesulfonimide (Li-TFSI) and other cobalt salts), is very sensitive to the experimental parameters used, since small deviations from the recommended quantities can drastically alter the performance. Furthermore, the presence of the dopants is thought to be responsible for the poor stability of the perovskite solar cell [18–20]. Spiro-OMeTAD needs to be doped by atmospheric oxygen, which temporally enhances the performance a few days (2–3) after the production of the solar cell [18–20]. For these reasons, and considering its relatively expensive cost, intense research efforts are on-going to find relevant HTM alternatives.

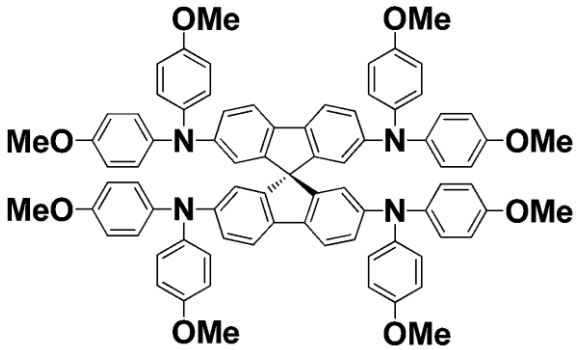

Figure 7. Spiro-OMeTAD.

5. Alternative π-Conjugated Materials for Hole Transport

5.1. Spiro-Core Small Molecules and Inspired Molecules

Since the Spiro-OMeTAD is known to be a good hole selective material, other Spiro-core molecules have been investigated in the field of perovskite solar cells. A molecule based on a Spiro-cyclopenta[2,1-*b*:3,4-*b*′]dithiophene (spiro-CPDT) connected by p-methoxy-substituted triphenylamine groups has been tested without dopant and reached fairly good performances [21]. The main issue with these molecules relates to their absorption peak in the blue region of the solar spectrum (between 400 and 500 nm), whereas Spiro-OMeTAD starts absorbing in the near UV region (below 400 nm). This leads to a dramatic reduction of the external quantum efficiency from the incident light reflected on the metallic top electrode. The hole mobility of this molecule, calculated by the space-charge limited current method, is about 6.0 × 10^{-6} cm^2· V^{-1}· s^{-1}. These molecules have been used on direct perovskite solar cells based on TiO_2. Without doping, these spiro-core molecules reached a mean power conversion efficiency (PCE) of 13.2%, while the Spiro-OMeTAD, doped with tBP, Li-TFSI and the cobalt complex FK209, obtained 10.3%.

Tetra{4-[*N*,*N*-(4,4′-dimethoxydiphenylamino)]phenyl}ethane (TAE-1) is a molecule very similar to Spiro-OMeTAD. The only difference is the presence of two double bonds replacing the double simple liaison at the center of the molecule. This molecule, used un-doped in a direct device architecture, allowed reaching a PCE of 11% [22].

In the family of molecules inspired by Spiro-OMeTAD, tetrakis[(4-me-thoxyphenyl)aminophenyl] ethane (etheneTTPA) is a molecule where the two typical single bonds at the center of Spiro-OMeTAD are replaced by a unique double bond [23]. This HTM was used in perovskite-sensitized TiO_2 solar

cells. The average J_{SC} was measured at 21.29 mA· cm^{-2} and the average V_{OC} at 0.91 V; the Fill Factor (FF) was 65% for a mean efficiency of 12.59%. After 200 h of illumination (conditions not specified), the solar cell with EtheneTTPA as HTL lost 36% of its initial efficiency. Unfortunately, no comparison with the Spiro-OMeTAD was reported. Finally, etheneTTPA can been seen as the assembly of two similar molecules of bis[(4-methoxyphenyl)aminophenyl]ethane (EtheneDTPA), which was also investigated and gave a mean efficiency of 10.26%.

5.2. EDOT-Core Small Molecules

In the same way, as it is possible to build molecules from a Spiro-core, it is also conceivable to do the same with an ethylenedioxythiophene (EDOT) core. Such a demonstration was carried out using TiO_2-based perovskite-sensitized solar cells (a direct device architecture), leading to promising results [24]. The champion cell was able to produce a J_{SC} of 21.07 mA· cm^{-2} with a V_{OC} of 0.947 V for an overall PCE of 14.23%, which is found to be comparable to that associated with the Spiro-OMeTAD reference cell (14.55%). This molecule appears to be slightly less stable than Spiro-OMeTAD, however. After constant illumination under 30 suns during 200 h, the perovskite solar cell based on the EDOT-core HTM lost 12% of its efficiency (7% loss for the Spiro-OMeTAD).

5.3. Substituted Carbazoles and Derivatives

One derivative of the carbazole unit is the poly(4,40-bis(*N*-carbazolyl)-1,10-biphenyl) (PPN) polymer. This polymer has been used as a 9 nm-thick HTL of a perovskite solar cell based on $CH_3NH_3PbI_3$ in an inverted device architecture and with C_{60} as the electron transport layer [25]. In this configuration, the PPN HTL allowed an open-circuit voltage of 970 mV, a short-circuit current density of 19.7 mA· cm^{-2}, a fill factor of 66% and a PCE of 12.8%, while the reference cell with a PEDOT:PSS HTL reached only a PCE of 11% and a low of V_{OC} of 790 mV. This difference was attributed to a better energetic configuration of the PPN HTL (ionization potential of −5.3 eV *vs.* vacuum) compared to Spiro-OMeTAD, which led to a more hole-selective contact.

Another serious candidate reported in the recent literature for the replacement of Spiro-OMeTAD is the methoxydiphenylamine-substituted carbazole twin derivative (referred to as V886) [26]. These small molecules are easily synthetized from a reaction of 1,2-bis(bromomethyl)benzene with 3,6-dibromocarbazole, followed by a palladium-catalyzed C–N cross coupling reaction with 4,4′-dimethoxydiphenylamine. This hole transporting material has been tested on the classical $CH_3NH_3PbI_3$ perovskite solar cell containing FTO and mesoporous TiO_2 as the photo anode. Compared to the best reference cell (PCE of 18.36%), the V886-based device showed a maximum power conversion efficiency of 16.91%. A high fill factor was also reported (73%), as well as a high photocurrent density of 21.38 mA· cm^{-2}, an open-circuit voltage of 1.085 V and very low hysteresis. It is interesting to note than V886 is soluble in THF and chlorobenzene. Furthermore, to achieve the suitable conductivity level, V886 was oxidized using, for example, FK209 (cobalt(III) complex). In this way, a conductivity of 4.2 × 10^{-5} S· cm^{-1}, comparable to that of Spiro-OMeTAD, was measured. One important advantage of this molecule is the simplicity of its synthesis.

Another member of the carbazole family is 8,16-didodecyl-8,16-dihydrobenzo[a]benzo[6,7]indolo [2,3-h]carbazole, named C12-Carbazole. A perovskite solar cell based on a direct architecture using the $CH_3NH_3PbI_3$ perovskite (synthesized using a two-step sequential deposition procedure) has shown a short-circuit current density of 21.13 mA· cm^{-2} and an open circuit tension of 860 mV, resulting in a power conversion efficiency of 11.26% for a fill factor of 62% [27]. Such relevant results remain to be more systematically reproduced, considering that the corresponding reference cell based on Spiro-OMeTAD was associated with a PCE of 9.62% only and a very low FF of 47%. Although such results raise the question of proper device characterization and optimization stage, this result shows the strong potentialities of this class of carbazole derivatives.

The research efforts on the carbazole family explored a large variety of possibilities. One of the strategies is finally to exploit small molecules with a carbazole-based arm linked together by a core

moiety [28]. To these carbazole arms were added flexible hexyloxy groups to enhance the solubility of the molecule in chlorobenzene, which is often used as solvent for the Spiro-OMeTAD. Following this strategy, a family of functional small molecules (noted as SGT-409, SGT-410, and SGT-411) were tested in a direct architecture. The best perovskite cell was obtained using the SGT-411 molecule as the HTM and demonstrated an efficiency of 13%, compared to 13.76% for the Spiro-OMeTAD reference solar cell. SGT-411 is, in terms of electronic properties, very close to the Spiro-OMeTAD. It is associated with a charge transfer kinetics in the order of 1.8 ns measured by time-resolved photoluminescence, compared to 1.3 ns for the Spiro-OMeTAD (when the SGT-409 and SGT-410 exhibit, respectively, 5.1 ns and 3.5 ns).

5.4. Tri-Phenylamine Derivatives

Diacetylide-triphenylamine (DATPA) derivatives were first tried as HTM in ssDSSC with the organic D102 dye [29], where they showed encouraging efficiency of 1.16% against 2.96% for the cell with the Spiro-OMeTAD. In the field of perovskites solar cells, two kinds of DATPA derivatives have been associated with significant performance so far: the Me_2N-DATPA and the MeO-DATPA, where Me_2N and MeO are $N(CH_3)_2$ and OCH_3 groups, respectively [30]. These molecules can form 2D sheets contacted with N-N bonds, with their HOMO extending across the whole molecule, enabling efficient hole transport. These molecules have the benefit of a much easier synthesis than Spiro-OMeTAD. Solar cells were prepared with an FTO/compact TiO_2/mesoporous Al_2O_3 scaffold/$CH_3NH_3PbI_{3-x}Cl_x$/HTM/Ag architecture, and the HTM doping was made with the protic bis(trifluoromethanesulfonyl)imide ionic liquid (which does not require oxygen exposure) and the tetraethyl bis-(trifluoromethane) sulfonamide salt, for both the DAPTA molecules and Spiro-OMeTAD. The reference cells, with Spiro-OMeTAD, had a mean efficiency of 10.6%, with a V_{OC} of 1.03 V, a J_{SC} of 19.52 mA$\cdot$ cm^{-2} and an FF of 57%; the MeO-DATPA cell had a mean efficiency of 5.9%, a V_{OC} of 0.99 V, a J_{SC} of 12.4 mA$\cdot$ cm^{-2} and an FF of 50%, while the Me_2N cell was found to be 5.7% efficient, with a V_{OC} of 0.87 V, a J_{SC} of 14.99 mA$\cdot$ cm^{-2} and an FF of 44%. These performances remain quite promising, considering the fact that the doping of Spiro-OMeTAD is now quite well optimized.

5.5. Phthalocyanine

Boron subphthalocyanine (SubPc) has been tested in a direct perovskite solar cell, using a vacuum process for its deposition [31]. During the first nine days after the production of the best cell, the J_{SC} and the FF increased from 14.0–21.3 mA$\cdot$ cm^{-2} and 40%–46%, respectively, while the V_{OC} decreased from 0.60 down to 0.37 V, resulting in a PCE evolving from 3.4%–6.6%. This evolution has already been observed for Spiro-OMeTAD and is normally attributed to its doping by atmospheric oxygen [18–20]. In reality, it seems that other mechanisms directly associated with the perovskite layer also play a role in this evolution.

Copper phthalocyanine (CuPc) is also a very well-known organic small molecule used for a decade in the field of organic field-effect transistors (OFET) as a *p*-type semiconductor [32–34]. It had been used for perovskite solar cells in 2012 [35] as an evaporated hole transporting layer, owing to the high charge mobility (up to 0.02 cm$^2\cdot$ V$^{-1}\cdot$ s^{-1}) associated with its high crystallinity. However, as it forms a large π-conjugated system, it remains difficult to dissolve in common organic solvents. Perovskite solar cells with an active area of 15 mm^2 based on a CuPc HTL and a classical TiO_2 ETL have demonstrated an average PCE of 3.7% with a J_{SC} of 14.7 mA$\cdot$ cm^{-2}, a V_{OC} of 0.71 V and an FF of 40% (the best cell showed a 5% PCE). The main drawback of this approach is clearly associated with a poor FF. Moreover, the absorption spectrum of CuPC is found suitable for the inverted architecture only, but it would not be possible to use it in a direct configuration. Indeed, a fraction of the light is normally reflected back in the perovskite layer by the metal electrode; this phenomenon can enhance the performance. In this case, the reflected light back would be absorbed by the Cu-phthalocyanine layer (Figure 8).

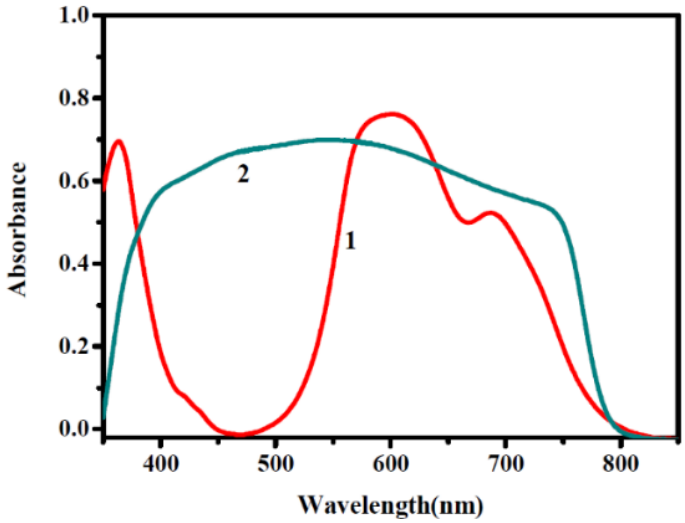

Figure 8. UV-VIS absorption spectra of (**1**) copper phthalocyanine (CuPc) thin film and (**2**) $TiO_2/CH_3NH_3PbCl_xI_{3-x}$ film. Reproduced from [35] with permission of The Royal Society of Chemistry.

5.6. Poly-TPD

The first use of poly(*N*,*N*′-bis(4-butylphenyl)-*N*,*N*′-bis(phenyl)benzidine (Poly-TPD) as a supplementary hole-transporting layer was initially reported at the interface between the conventional PEDOT:PSS HTL and the $CH_3NH_3PbI_3$ perovskite in order to better match the perovskite valence band (the ETL was PCBM in this case). At this time, this cell reached 12% efficiency, but this performance was characterized by a relatively low current density of 16 mA· cm^{-2} [15]. A few months later, the same team successfully used Poly-TPD alone as HTM, but this time with a co-evaporated perovskite absorber, a technique that allows producing a high-quality perovskite layer [36]. In an attempt to produce a large active area, two surfaces were tested: 0.065 cm^2 and 0.95 cm^2. The associated photovoltaic parameters are summarized in the Table 2. As we can see, it appears highly challenging to enlarge the active surface area while preserving a good fill factor: statistically, the larger the surface, the larger the number of defaults, the smaller the fill factor. The first solution-processed perovskite solar cells with only Poly-TPD was produced in late 2014 and demonstrated a mean efficiency of 13.78% (V_{OC} = 0.99) [37]. From the SEM images of the perovskite layer deposited on the HTL (Figure 9), we observe that the grain size of the perovskite on the Poly-TPD is much larger than on PEDOT:PSS, resulting in a higher FF. Even if these performances with Poly-TPD as HTL are very good, these are to be considered with regard to the quite low performance of the reference PEDOT:PSS device (only 4.7% for the PCE), instead of the usual state-of-the-art performance (around 15%). Nevertheless, the true advantages of Poly-TPD are associated with its ability to form high quality films from spin coating, as well as a relatively reduced annealing temperature of 110 °C (for 30 min).

Table 2. Photovoltaic parameters summary for the perovskite cells based on a poly(*N*,*N*′-bis(4-butylphenyl)-*N*,*N*′-bis(phenyl)benzidine (Poly-TPD) hole transport layer (HTL) [35].

Active Surface Area (cm^2)	η (%)	J_{SC} (mA· cm^2)	V_{OC} (V)	FF (%)
0.065	14.8	18.2	1.09	75
0.95	10.9	17.9	1.07	57

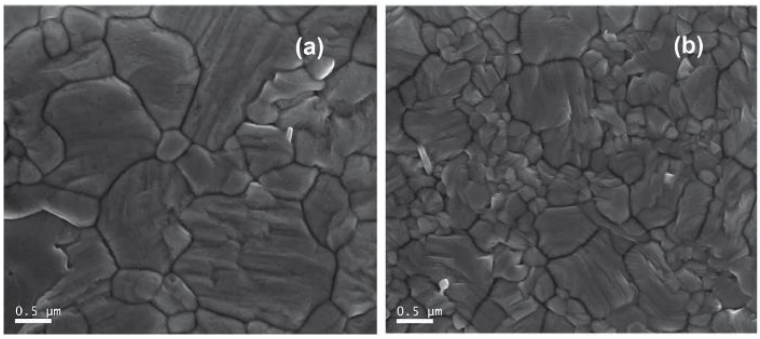

Figure 9. SEM images of a perovskite film deposited on a (**a**) Poly-TPD and (**b**) PEDOT:PSS underlying HTL. Reproduced from [37] with permission of The Royal Society of Chemistry.

5.7. PTAA Derivatives

In order to reduce the series resistance of solar cells based on PEDOT:PSS HTL, poly(triarylamine) (PTAA), which was already demonstrated as an efficient hole transporter in the field of solid-state dye-sensitized solar cells, has been tested with 2,3,5,6-tandrafluoro-7,7,8,8-tandracyanoquinodimandhane (F4-TCNQ) as a dopant [38]. In this investigation it is important to note that 4,4′,4″-tris[phenyl(m-tolyl)amino]triphenylamine (m-MTDATA) has been added (at ~10 wt. %) to help the wetting on ITO. The objective of this study was to identify the influence of the dopant on the photovoltaic performance of the cell. The perovskite layer ($CH_3NH_3PbI_3$) has been deposited with a two-step method, by spin-coating a PbI_2 solution in DMF, followed by another spin coating cycle of methylammonium iodide in DMF, before a final annealing at 100 °C under saturated DMF vapor in air. The resulting photovoltaic parameters are summarized in the Table 3. The main effect of the dopant is to drastically improve the conductivity of the HTL, leading to a reduction of the series resistance of the device, hence to an enhancement of the fill factor of the cell. An impressive power conversion efficiency over 17% is demonstrated in this case.

Table 3. Summary of photovoltaic performance from [38]. F4-TCNQ, 2,3,5,6-tandrafluoro-7,7,8,8-tandracyanoquinodimandhane; PCE, power conversion efficiency.

F4-TCNQ Ratio (wt. %)	J_{SC} (mA· cm^{-2})	V_{OC} (V)	FF (%)	PCE (%)	Series Resistance (Ω cm^2)
0	21.6	1.05	65.7	14.8	9.07
0.01	21.0	1.05	65.8	14.5	7.57
0.1	21.5	1.05	65.5	14.8	7.72
1	21.6	1.09	74.0	17.5	6.07
2	21.0	1.09	68.2	15.6	8.56
10	21.2	1.09	64.1	14.8	9.77

5.8. Polyelectrolytes

Another kind of hole transporting layer is based on conjugated polyelectrolytes, which have been employed for the first time in 2015 for perovskite solar cells, using CPE-K (poly[2,6-(4,4-bis-potassiumbutanylsulfonate-4*H*-cyclopenta-[2,1-*b*;3,4-*b*′]-dithiophene)-alt-4,7-(2,1,3-benzothiadiazole)]) [39]. The transmittance spectra of this polyelectrolyte is lower than the one of PEDOT:PSS (Figure 10) and is sensitive to the DMF solvent of the perovskite. This polymer was tested with the $CH_3NH_3PbI_{3-x}Cl_x$ mixed halide perovskites, leading to a champion cell presenting an efficiency of 12.51%, with regard to the 10.77% achieved for the PEDOT:PSS reference solar cell (with a voltage of 0.89 V against 0.84 V, a J_{SC} of 20.10 mA· cm^{-2} against 19.58 mA· cm^{-2} and an FF of 77% against 66%). The average performance were reported at 11.20% and 9.37%, respectively. CPE-K seems to give a better stability under air and light illumination: after a 12-h exposure to air, the performance of the PEDOT:PSS cells dropped down to almost 0% after 40 min only of sun light exposure, while this

drop is observed after 120 min for the CPE-K cell. This phenomenon could be explained by the acidity of the PEDOT:PSS, which can be detrimental to the perovskite layer.

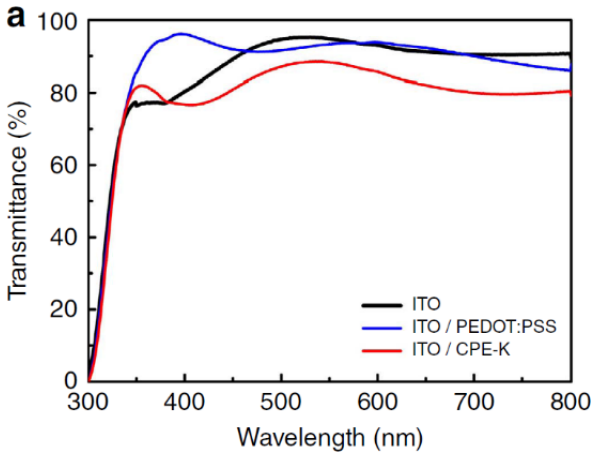

Figure 10. Comparison of the transmittance between PEDOT:PSS and CPE-K (poly[2,6-(4,4-bis-potassiumbutanylsulfonate-4*H*-cyclopenta-[2,1-*b*;3,4-*b*′]-dithiophene)-alt-4,7-(2,1,3-benzothiadiazole)]) on the ITO substrate [39].

P3CT-Na is another polyelectrolyte tested in 2015, which has a higher work function than PEDOT:PSS (5.11 eV for PEDOT:PSS on ITO and 5.26 for P3CT-Na in the same conditions) that lies closer to the valence band of the perovskites [40]. This polyelectrolyte is water soluble and can be directly spin coated on the ITO. For a thickness of 4 nm, a mean efficiency of 16.6% is obtained, illustrating the relevance of this strategy for efficient perovskite solar cells.

5.9. Thiophene Derivative

As a replacement of PEDOT:PSS, the simple polythiophene (PT) polymer was successfully investigated on the inverted device architecture. Using an optimum thickness of 6 nm, these PT-based cells achieved a mean efficiency of 14.7% [25], compared to the relative low (11%) efficiency of the reference PEDOT:PSS cell. Such results show that PT can indeed work as efficient hole transporters. Some variations were explored using a silolothiophene linked to a methoxy triphenylamine molecule, which aimed at improving the stability of the device. From this strategy, two molecules, named PEH-1 and PEH-2, have been tested on inverted perovskite solar cells [41]. They differ by the nature of the organic side groups attached to the silicon atom in the silolothiophene unit. The best performance was observed with the PEH-2 HTM, bearing two phenyl rings, with a PCE of 13.5%, while the PEH-1 (bearing two hexyl chains) was at 11.7%, the reference cell PCE being at 15.2%. Interestingly, the authors evidence a correlation between the slow component of the degradation kinetics and the nature of the HTM. After 200 h under illumination, the PEH-2 cell lost approximately 7% of its initial efficiency, while the Spiro-OMeTAD cell exhibited an almost 20% loss. After 875 h of illumination, the PEH-2 cell kept a little more than 60% of its efficiency, while the reference cell fell down to 45% of its initial PCE. The authors interpret these data by inferring that the decay in performance is supposedly due to the formation of shunting pathways caused by metal electrode migration within the HTM and contacting the perovskite layer.

5.10. Phenylene Derivative

The electropolymerized poly(p-phenylene) (PPP) polymer was found to be a viable alternative to PEDOT:PSS. With the benefit of its insolubility in DMF, a high mean efficiency of 15.8% was achieved in 2015, with a V_{OC} of 1.02 V and a J_{SC} of 21 mA$\cdot$cm^{-2}, the champion cell reaching even a PCE of 16.5% [25]. Associated with a very smooth surface, the PPP film had a thickness of 11 nm and shows a

ten-times higher recombination resistance (as measured by electrochemical impedance spectroscopy) than that measured on PEDOT:PSS (7×10^6 Ω against 8×10^5 Ω).

5.11. Furan-Based Small Molecule

In order to achieve a better π stacking of the molecular glass and a better pore filling of the mesoporous TiO_2, a relevant strategy is to choose a smaller and more planar molecule. In this context, furan-based molecules are highly relevant, as the presence of an oxygen atom instead of sulfur generally leads to reaching these objectives. Moreover, such molecules are compatible with shorter and less expensive synthesis than that of Spiro-OMeTAD. An example was reported in 2015, by coupling a furan core to tri-arylamine groups, leading to the F101 molecule [42]. Its optical absorption is only slightly red shifted compared to that of Spiro-OMeTAD. The molecule has been tested on a direct architecture cell based on the $CH_3NH_3PbI_3$ perovskite, produced by the two-step method. While the reference cell with Spiro-OMeTAD reached 13.1% in efficiency with an open-circuit of 1.05 V and a relatively low short-circuit current density of 18.4 mA·cm^{-2}, the cell with F101 performed similarly, with an average PCE of 13.1%, a V_{OC} of 1.1 V and a J_{SC} of 19.63 mA·cm^{-2}. The main difference between these two cells is a lower FF (61%) for the F101 compared to the 68% FF of the reference cell. Finally, it is important to note that the Spiro-OMeTAD and the F101 were doped with $Li(CF_3SO_2)_2N$, *tert*-butylpyridine and tris[2-(1*H*-pyrazol-1-yl)pyridine]cobalt(III).

5.12. HOMO and LUMO Levels of the Reviewed Materials

In order to easily find the HOMO and LUMO level energy of the reviewed materials, please refer to Table 4, which summarizes these energy values for several HTMs in perovskite solar cells and for respective solar cell efficiencies exceeding 10%.

Table 4. HOMO and LUMO levels of some HTMs and of the perovskites. EtheneTTPA, tetrakis[(4-me-thoxyphenyl)aminophenyl]ethane; TAE-1, Tetra{4-[*N*,*N*-(4,4′-dimethoxydiphenylamino)]phenyl}ethane; SubPc, subphthalocyanine.

Material	MeN-datpta	CPE-K	EtheneTTPA	MeO_2-datpa	PEH-1	PEH-2	F101	CuPc	C12 Carbazole	PEDOT:PSS	Spiro-OMeTAD	$MAPbI_{3-x}Cl_x$	$MAPbI_3$	Poly-TPD	TAE-1	SubPc
HOMO	−1.79	−3.50	/	−2.29	−2.73	−2.8	−2.40	−3.5	/	−3.00	−2.05	−3.75	−3.93	−2.40	−2.74	−3.60
LUMO	−4.4	−4.90	−5.02	−5.02	−5.16	−5.17	−5.18	−5.2	−5.29	−5.20	−5.22	−5.3	−5.43	−5.40	−5.44	−5.60

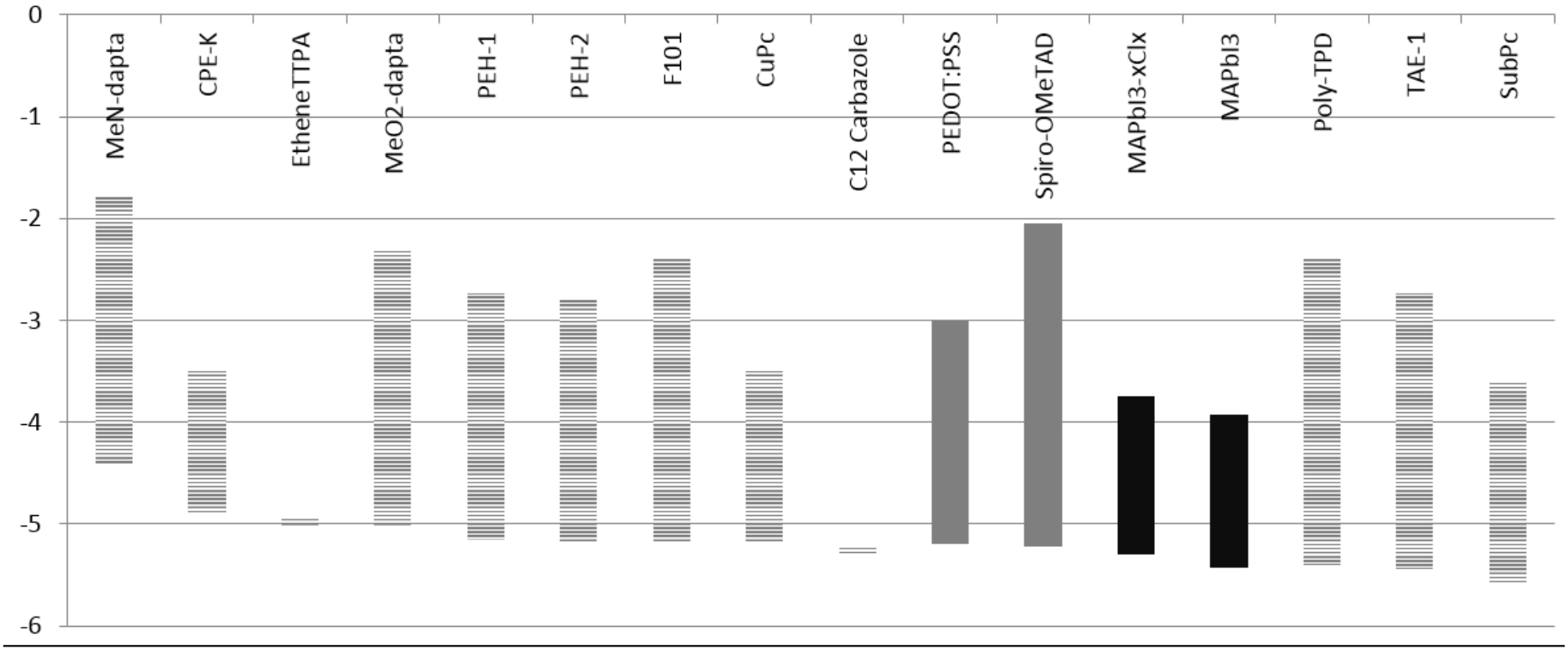

6. Discussion and Perspectives

This overview of the recent developments of organic hole conductors for perovskite solar cells highlighted the main features required for any efficient HTM alternative to the Spiro-OMeTAD or PEDOT:PSS reference materials. Table 5 summarizes this non-exhaustive list, based on the most significant approaches that were mainly developed in 2015, including the type of device architecture and the photovoltaic parameters that were explored.

In these attempts to design new HTMs for perovskite solar cells, a large variety of molecules and polymers have been synthesized and proposed. In all cases, researcher have to deal with advantages, drawback and peculiarities. Considering the large number of structures that have been reported in the last five years, it remain highly challenging, in our opinion, to predict the next organic compound that will compete with the current references materials. Anyhow, we emphasize, from our physico-chemist point of view, a number of common issues associated with the development of efficient HTM. First of all, they are all yet to be optimized, through doping and processing. This aspect is very important considering that Spiro-OMeTAD has been now used for a decade, making it a very well-known system that is difficult to replace. This issue reveals also a contradiction in the research for new hole transport materials. Indeed, this review evidences that a relatively high number of viable alternatives to Spiro-OMeTAD or PEDOT:PSS are demonstrated today, but none of them actually replace these two classical HTMs, as none of these new HTMs are in fact fully optimized to a specific device architecture and active material. Secondly, only a few of these new HTMs have been assessed in terms of stability, which is of course crucial if we want to design efficient and robust materials for the new generation of solar cells. A thoroughly-optimized HTM is indeed an important element to obtain a device that shows a very good stability. The nature of the HTM plays also an important role in the stability of the perovskite layer itself [43]. Thirdly, as these new HTM ought to be used in affordable solar cells, they have to be compatible with low-cost deposition technologies, such as printing. Therefore, the true potential of any newly-designed HTM can only be identified if it is also tested in terms of printability.

Finally, all of these HTMs should be now tested on larger active area, closer to the standards generally considered in the photovoltaic community. Indeed, additional defects and issues generally arise when going to a larger area, which make it difficult to properly distinguish today's materials that are compatible with such a scale-up. In this context, we also emphasize a specific aspect associated with device characterization, which has a strong influence on the reported efficiencies. Apart from the necessity to use a suitable protocol for device testing to avoid any artefacts due to the presence of hysteresis or to the influence of the electrical scan parameters [44], particular attention needs to be paid to the definition of the active area of the considered device. Such a parameter is crucial in the context of HTM developments, as it can greatly distort the reported efficiency of a specific material with regard to another. As an example, we plot the power conversion efficiency of the cells reviewed in this article as a function of active area (Figure 11).

Although there is no possible correlation between the different studies described in this review, it seems that the most efficient demonstrations are associated with a small active area (<10 mm^2). Apart from the fact that performance is statistically less dependent on the occurrence of defects on a small area, a larger active area is associated with larger ohmic losses due to the transparent electrodes and various interlayers, making any direct comparisons difficult. Such a problem is a general issue in the field of third generation photovoltaic cells, but any occasion is relevant to point out its strong influence on interpretations. Consequently, the comparison between HTMs has to be always considered in regard to the apparent correlation between active area size and performance.

We point out that the nature of the ETL, either for direct or inverted device architectures, is of particular importance for efficient device operation. Although this aspect remains out of the scope of our review, we refer the reader to recent articles especially devoted to this aspect [45–48].

Table 5. Summary of the different HTMs developed in the last few years for perovskite solar cells and the photovoltaic parameters of the corresponding champion cells, as measured under 100 mW· cm^{-2} under the AM1.5G solar spectrum. For clarity, only the data associated with PCE exceeding results 10% have been considered. The P3CT-Na figure was reproduced from [40] with permission of The Royal Society of Chemistry. spiro-CPDT, Spiro-cyclopenta[2,1-*b*:3,4-*b*′]dithiophene; EDOT, ethylenedioxythiophene; PPN, poly(4,40-bis(*N*-carbazolyl)-1,10-biphenyl); PT, polythiophene; PPP, poly(*p*-phenylene); PTAA, poly(triarylamine).

Hole Transport Material Name	Representation	Molecule Family	Tested Perovskite Solar Cell	Best V_{OC} (mV)	Best J_{SC} (mA· cm^{-2})	Best Fill Factor (%)	Best PCE (%)	Surface Area (cm^2)	Reference
Spiro-OMeTAD		Spiro Core	Indirect	1130	22.75	75.01	19.3	0.1	[10]
PEDOT:PSS		EDOT Core	Direct	1100	20.9	79	18.2	0.096	[17]
Spiro-CPDT	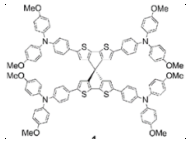	Spiro Core	Direct	971	19.3	72	13.4	0.16	[20]
TAE-1	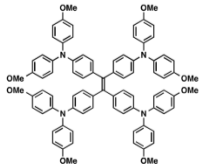	Spiro Inspired	Direct	885	17.22	72	11.00	?	[21]
EtheneTTPA	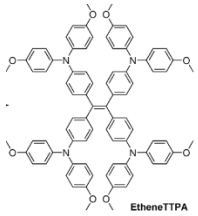	Spiro Inspired	Direct	920	21.24	67	13.09	0.16	[22]
PPN	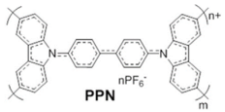	Carbazole	Inverted	990	20.1	72	14.3	?	[24]
V886	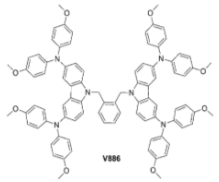	Carbazole	Direct	1085	21.38	73	16.91	0.16	[25]

Table 5. *Cont.*

Hole Transport Material Name	Representation	Molecule Family	Tested Perovskite Solar Cell	Best V_{OC} (mV)	Best J_{SC} (mA· cm^{-2})	Best Fill Factor (%)	Best PCE (%)	Surface Area (cm^2)	Reference
C12-Carbazole	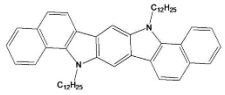	Carbazole	Direct	860	21.13	62	11.26	?	[26]
SGT-409	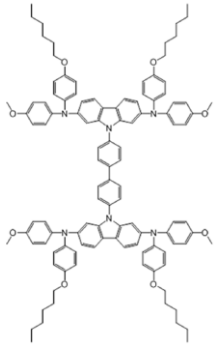	Carbazole	Direct	938	18.63	63	10.93	0.30	[27]
SGT-410	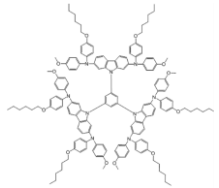	Carbazole	Direct	984	18.55	67	12.61	0.30	[27]
SGT-411	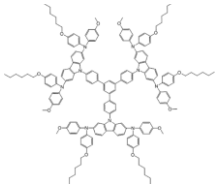	Carbazole	Direct	997	18.60	67	13.00	0.30	[27]
CPE-K	-	Polyelectrolyte	Inverted	890	20.1	77	12.51	0.033	[38]
P3CT-Na	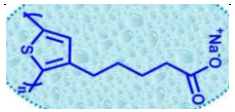	Polyelectrolyte	Inverted	1070	21.14	73	16.6	0.09	[29]

Table 5. *Cont.*

Hole Transport Material Name	Representation	Molecule Family	Tested Perovskite Solar Cell	Best V_{OC} (mV)	Best J_{SC} (mA· cm^{-2})	Best Fill Factor (%)	Best PCE (%)	Surface Area (cm^2)	Reference
PT	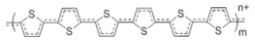	Thiophene	Inverted	960	21.8	78	16.1	?	[24]
PEH-1	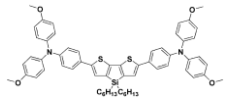	Thiophene	Direct	960	16.8	72	11.7	0.16	[40]
PEH-2	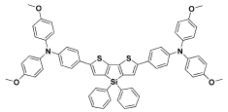	Thiophene	Direct	970	19.4	72	13.5	0.16	[40]
PPP		Phenylene	Inverted	1020	21.0	71	15.8	?	[24]
F101	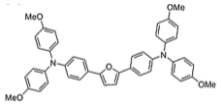	Furan	Direct	1100	19.63	61	13.1	0.2	[41]
DPEDOT-B[BMPDP	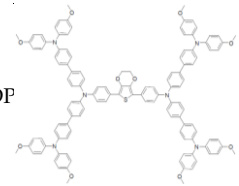	EDOT-Core	Direct	951	20.96	70	14.00	0.16	[23]
Poly-TPD	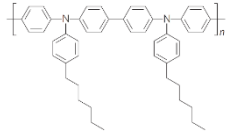	-	Inverted	1090	18.2	75	14.3	0.065	[35]
PTAA	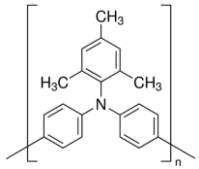	-	Inverted	1090	21.6	74	17.5	?	[37]

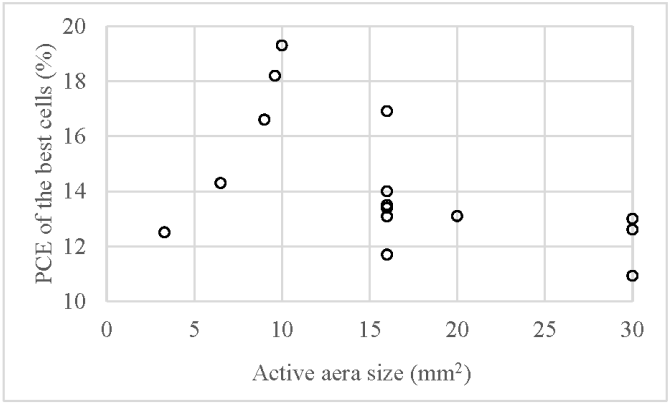

Figure 11. Relation between active area size and overall performance of perovskite solar cells reviewed in this work (all cells are characterized under AM1.5 illumination, 100 mW· cm^{-2}).

7. Conclusions

In this review, we focused on the recent developments of organic hole transport materials (HTMs) in the field of hybrid perovskite solar cells. We especially emphasized the relationships between high efficiencies and HTM physico-chemical properties, such as optical properties, thermal properties or rheological properties. We also pointed out the importance of the perovskite/HTM interface on device operation, through considerations of the relations between the surface tension of HTM precursor solutions and the surface energy of the perovskite layer. Our synthetic description of the most recent achievements in the design of HTM for perovskite solar cells highlights the large number of potential candidates, which allows the demonstration of devices presenting power conversion efficiencies over 10%.

Benefiting from developments made in the field of organic and dye-sensitized solar cells, perovskite devices are now driving a highly dynamic research community towards the synthesis of high mobility compounds presenting increasing stability. However, although numerous materials are now capable of achieving high performance, there are only a few HTMs that have actually been tested over a large active area and over long periods of device operation in controlled conditions. Important efforts are also required to specifically evaluate HTM with regard to printing technologies, in order to confirm the strong potentialities of perovskite solar cells as a viable alternative for inexpensive and large area photovoltaic energy conversion.

Acknowledgments: The authors would like to thank their two financers: the Labex Σ-Lim and the French ministry of defense's DGA.

Author Contributions: All the authors participated in the initial structuration of the article. A.G. performed the few experiments described in the paper, directly supervised by S.V., B.R., and J.B., and also wrote the initial version of the review. A.G., S.V, B.R. and J.B. contributed equally to the correction of the draft towards the final version.

Conflicts of Interest: The authors declare no conflict of interest.

References

1. Gao, P.; Grätzel, M.; Nazeeruddin, M.K. Organohalide lead perovskites for photovoltaic applications. *Energy Environ. Sci.* **2014**, *7*, 2448–2463. [CrossRef]
2. Green, A.M.; Ho-Baillie, A.J.; Snaith, H. The emergence of perovskite solar cells. *Nat. Photonics* **2014**, *8*, 506–514. [CrossRef]
3. Even, J.; Pedesseau, L.; Katan, C.; Kepenekian, M.; Lauret, J.S.; Sapori, D.; Deleport, E. Solid-State Physics Perspective on Hybrid Perovskite. *J. Phys. Chem. C* **2015**, *119*, 10161–10177. [CrossRef]
4. Wehrenfennig, C.; Eperon, G.E.; Johnston, M.B.; Snaith, H.J.; Herz, L.M. High Charge Carrier Mobilities and Lifetimes in Organolead Trihalide Perovskites. *Adv. Mat. Res.* **2013**, *26*, 1584–1589. [CrossRef]

5. Chynoweth, A.G. Surface Space-Charge Layers in Barium Titanate. *Phys. Rev.* **1656**, *102*, 705–714. [CrossRef]
6. Kojima, A.; Teshima, K.; Shirai, Y.; Miyasaka, T. Novel Photoelectrochemical Cell with Mesoscopic Electrodes Sensitized by Lead-halide Compounds. In Proceedings of the 212th ECS Meeting, Washington, DC, USA, 7–12 October 2007.
7. Kojima, A.; Teshima, K.; Shirai, Y.; Miyasaka, T. Organometal Halide Perovskites as Visible-Light Sensitizers for Photovoltaic Cells. *J. Am. Chem. Soc.* **2009**, *131*, 6050–6051. [CrossRef] [PubMed]
8. Kim, H.S.; Lee, C.R.; Im, J.H.; Lee, K.B.; Moehl, T.; Marchioro, A.; Moon, S.J.; Humphry-Baker, R.; Yum, J.H.; Moser, E.J.; *et al*. Lead Iodide Perovskite Sensitized All-Solid-State Submicron Thin Film Mesoscopic Solar Cell with Efficiency Exceeding 9%. *Sci. Rep.* **2012**, *2*, 591. [CrossRef] [PubMed]
9. Lee, M.M.; Teuscher, J.; Miyasaka, T.; Murakami, T.N.; Snaith, H.J. Efficient Hybrid Solar Cells Based on Meso-Superstructured Organometal Halide Perovskites. *Science* **2012**, *338*, 643–647. [CrossRef] [PubMed]
10. Zhou, H.; Chen, Q. Interface engineering of highly efficient perovskite solar cells. *Science* **2014**, *354*, 542–546. [CrossRef] [PubMed]
11. Salim, T.; Sun, S.; Abe, Y.; Krishna, A.; Grimsdale, A.C.; Lam, Y.M. Perovskite-based solar cells: Impact of morphology and device architecture on device performance. *J. Mater. Chem. A* **2014**, *3*, 8943–8969. [CrossRef]
12. Völker, S.; Delgado, J.L. Organic Charge Carriers for Perovskite Solar Cells. *ChemSusChem* **2015**, *8*, 3012–3028.
13. Yu, Z.; Sun, L. Recent Progress on Hole-Transporting Materials for Emerging Organometal Halide Perovskite Solar Cells. *Adv. Energy Mater.* **2015**. [CrossRef]
14. Jeng, J.Y.; Chiang, Y.F.; Lee, M.H.; Peng, S.R.; Guo, T.F.; Chen, P.; Wen, T.C. $CH_3NH_3PbI_3$ Perovskite/Fullerene Planar-Heterojunction Hybrid Solar Cells. *Adv. Mater.* **2013**, *25*, 3727–3732. [CrossRef] [PubMed]
15. Sun, S.; Salim, T.; Mathews, N.; Duchamp, M.; Boothroyd, C.; Xing, G.; Sum, T.C.; Lam, Y.M. The origin of high efficiency in low-temperature solution-processable bilayer organometal halide hybrid solar cells. *Energy Environ. Sci.* **2013**, *7*, 399–407. [CrossRef]
16. Malinkiewicz, O.; Yella, A.; Lee, Y.H.; Espallargas, G.M.; Graetzel, M.; Nazeeruddin, M.K.; Bolink, H.J. Perovskite solar cells employing organic charge-transport layers. *Nat. Photonics* **2013**, *8*, 128–132. [CrossRef]
17. Docampo, P.; Ball, J.M.; Eperon, G.E.; Snaith, H.J. Efficient organometal trihalide perovskite planar-heterojunction solar cells on flexible polymer substrates. *Nat. Commun.* **2013**. [CrossRef] [PubMed]
18. Heo, J.H.; Han, H.J.; Kim, D.; Ahn, T.K.; Im, S.H. 18.1% hysteresis-less inverted $CH_3NH_3PbI_3$ planar perovskite hybrid solar cells. *Energy Environ. Sci.* **2015**, *8*, 1602–1608. [CrossRef]
19. Sheikh, A.D.; Bera, A.; Hague, M.A.; Rakhi, R.B.; Gobbo, S.D.; Alshareef, H.N.; Wu, T. Atmospheric effects on the photovoltaic performance of hybrid perovskitesolarcells. *Sol. Energy Mater. Sol. Cells* **2015**, *137*, 6–14. [CrossRef]
20. Antoniadou, M.; Siranidi, E.; Vaenas, N.; Kontos, A.G.; Stathatos, E.; Falaras, P. Photovoltaic Performance and Stability of $CH_3NH_3PbI_{3-x}Cl_x$ Perovskites. *J. Surf. Interface Mater.* **2014**, *2*, 1–5.
21. Franckevicius, M.; Mishra, A.; Kreuzer, F.; Luo, J.; Zakeeruddin, S.M.; Gratzel, M. A dopant-free spirobi[cyclopenta[2,1-*b*:3,4-*b*′]-dithiophene] based hole-transport material for efficient perovskite solar cells. *Mater. Horiz.* **2015**, *6*, 613–618. [CrossRef]
22. Cabau, L.; Garcia-Benito, I.; Molina-Ontoria, A.; Montcada, N.F.; Martin, N.; Vidal-Ferran, A.; Palomares, E. Diarylamino-substituted Tetraarylethene (TAE) as Efficient and Robust Hole Transport Material for 11% Methyl Ammonium Lead Iodide Perovskite Solar Cells. *Chem. Commun.* **2015**, *51*, 13980–13982. [CrossRef] [PubMed]
23. Choi, H.; Do, K.; Park, S.; Yu, J.S.; Ko, J. Efficient Hole Transporting Materials with Two or Four *N*,*N*-di(4-methoxyphenyl)aminophenyl on Ethene Unit for Perovskite Solar. *Chem. Eur. J.* **2015**, *21*, 15919–12923. [CrossRef] [PubMed]
24. Choi, H.; Park, S.; Kang, M.S.; Ko, J. Efficient symmetric oligomer hole transporting materials with different cores for high performance perovskite solar cells. *Chem. Commun.* **2015**, *51*, 15506–15509. [CrossRef] [PubMed]
25. Yan, W.; Li, Y.; Li, Y.; Ye, S.; Liu, Z.; Wang, S.; Bian, Z.; Huang, C. High-performance hybrid perovskite solar cells with open circuit voltage dependence on hole-transporting materials. *Nano Energy* **2015**, *16*, 428–437. [CrossRef]
26. Gratia, P.; Magomedov, A.; Malinauskas, T.; Daskeviciene, M.; Abate, A.; Ahmad, S.; Grätzel, M.; Getautis, V.; Nazeeruddin, M.K. Methoxydiphenylamine Substituted Carbazole Twin Derivative: An Efficient Hole Transporting Material for Perovskite Solar Cells. *Angew. Chem.* **2015**, *54*, 11409–11413. [CrossRef] [PubMed]

27. Lim, I.; Kim, E.K.; Patil, S.A.; Ahn, D.Y.; Lee, W.; Shrestha, N.K.; Lee, J.K.; Seok, W.K.; Cho, C.G.; Han, S.H. Indolocarbazole based small molecule: An efficient hole transporting material for perovskite solar cells. *RSC Adv.* **2015**, *5*, 55321–55327. [CrossRef]
28. Kang, M.S.; Sung, S.D.; Choi, I.T.; Kim, H.; Hong, M.; Kim, J.; Kim, H.K. Novel Carbazole-Based Hole-Transporting Materials with Star-Shaped Chemical Structures for Perovskite-Sensitized Solar Cells. *Appl. Mater. Interfaces* **2015**, *7*, 22213–22217. [CrossRef] [PubMed]
29. Planells, M.; Abate, A.; Hollman, D.J.; Stranks, S.D.; Bharti, V.; Gaur, J.; Mohanty, D.; Chand, S.; Snaith, H.J.; Robertson, N. Diacetylene bridged triphenylamines as hole transport materials for solid state dye sensitized solar cells. *J. Mater. Chem. A* **2013**, *1*, 6949–6960. [CrossRef]
30. Abate, A.; Planells, M.; Hollman, D.J.; Barthi, V.; Chand, S.; Snaith, H.J.; Robertson, N. Hole-Transport Materials with Greatly-differing Redox Potentials give Efficient TiO_2-[CH_3NH_3][PbX_3] Perovskite Solar Cells. *Phys. Chem. Chem. Phys.* **2014**, *17*, 2335–2338. [CrossRef] [PubMed]
31. Sfyri, G.; Kumar, C.V.; Sabapathi, G.; Giribabu, L.; Andrikopoulos, K.S.; Stathatos, E.; Lianos, P. Subphthalocyanine as Hole Transporting Material for Perovskite Solar Cells. *RSC Adv.* **2015**, *5*, 69813–69818. [CrossRef]
32. Murphy, A.R.; Fréchet, J.M.J. Organic Semiconducting Oligomers for Use in Thin Film Transistors. *Chem. Rev.* **2007**, *107*, 1066–1096. [CrossRef] [PubMed]
33. Sun, Y.; Liu, Y.; Zhu, D. Advances in organic field-effect transistors. *J. Mater. Chem.* **2004**, *15*, 53–65. [CrossRef]
34. Zaumseil, J.; Sirringhaus, H. Electron and Ambipolar Transport in Organic Field-Effect Transistors. *Chem. Rev.* **2007**, *107*, 1296–1323. [CrossRef] [PubMed]
35. Kumar, C.V.; Sfyri, G.; Raptis, D.; Stathatos, E.; Lianos, P. Perovskite Solar Cell with Low Cost Cu-Phthalocyanine as Hole Transporting Material. *RSC Adv.* **2012**, *5*, 3786–3791. [CrossRef]
36. Malinkiewicz, O.; Roldán-Carmona, C.; Soriano, A.; Bandiello, E.; Camacho, L.; Nazeeruddin, M.K.; Bolink, H.J. Metal-Oxide-Free Methylammonium Lead Iodide Perovskite-Based Solar Cells: The Influence of Organic Charge Transport Layers. *Adv. Energy Mater.* **2014**. [CrossRef]
37. Zhao, D.; Sexton, M.; Park, H.Y.; Baure, G.; Nino, J.C.; So, F. High Efficiency Solution-Processed Planar Perovskite Solar Cells with a Polymer Hole Transport Layer. *Adv. Energy Mater.* **2014**. [CrossRef]
38. Wang, Q.; Bi, C.; Huang, J. Doped hole transport layer for efficiency enhancement in planar heterojunction organolead trihalide perovskite solar cells. *Nano Energy* **2015**, *15*, 275–280. [CrossRef]
39. Choi, H.; Jeong, J.; Song, S.; Bazan, G.C.; Kim, J.Y.; Heeger, A.J. Conjugated polyelectrolyte hole transport layer for inverted-type perovskite solar cells. *Nat. Commun.* **2015**. [CrossRef] [PubMed]
40. Li, X.; Liu, X.; Wang, X.; Zhao, L.; Jiu, T.; Fang, J. Polyelectrolyte Based Hole-Transporting Materials for High Performance Solution Processed Planar Perovskite Solar Cells. *J. Mater. Chem.* **2015**, *3*, 15024–15029. [CrossRef]
41. Abate, A.; Paek, S.; Giordano, F.; Correa-Baena, J.P.; Saliba, M.; Gao, P.; Matsui, T.; Ko, J.; Zakeeruddin, S.M.; Dahmen, K.H.; *et al*. Silolothiophene-linked triphenylamines as stable hole transporting materials for high efficiency perovskite solar cells. *Energy Environ. Sci.* **2015**, *8*, 2946–2953. [CrossRef]
42. Krishna, A.; Sabba, D.; Yin, J.; Bruno, A.; Boix, P.P.; Gao, Y.; Dewi, H.A.; Gurzadyan, G.G.; Soci, C.; Mhaisalkar, S.G.; *et al*. Facile Synthesis of a Furan-Arylamine Hole-Transporting Material for High-Efficiency, Mesoscopic Perovskite Solar Cells. *Chem. Eur. J.* **2015**, *21*, 1–6. [CrossRef] [PubMed]
43. Chen, W.; Wu, Y.; Yue, Y.; Liu, J.; Zhang, W.; Yang, X.; Chen, H.; Bi, E.; Ashraful, I.; Grätzel, M.; *et al*. Efficient and stable large-area perovskite solar cells with inorganic charge extraction layers. *Science* **2015**, *350*, 944–948. [CrossRef] [PubMed]
44. Christians, J.A.; Manser, J.S.; Kamat, P.V. Best Practices in Perovskite Solar Cell Efficiency Measurements. Avoiding the Error of Making Bad Cells Look Good. *J. Phys. Chem. Lett.* **2015**, *6*, 862–867. [CrossRef] [PubMed]
45. Wojciechowski, K.; Leijtens, T.; Siprova, S.; Schlueter, C.; Hörantner, M.T.; Wang, J.T.W.; Li, C.Z.; Jen, A.K.Y.; Lee, T.L.; Snaith, H.J. C60 as an Efficient *n*-Type Compact Layer in Perovskite Solar Cells. *J. Phys. Chem. Lett.* **2015**, *6*, 2399–2405. [CrossRef] [PubMed]
46. Lo, M.F.; Guan, Z.Q.; Ng, T.W.; Chan, C.Y.; Lee, C.S. Electronic Structures and Photoconversion Mechanism in Perovskite/Fullerene Heterojunctions. *Adv. Funct. Mater.* **2014**. [CrossRef]

47. Li, C.Z.; Liang, P.W.; Sulas, D.B.; Nguyen, P.D.; Li, X.; Ginger, D.S.; Schlenker, C.W.; Jen, A.K.Y. Modulation of hybrid organic-perovskite photovoltaic performance by controlling the excited dynamics of fullerenes. *Mater. Horiz.* **2015**, *2*, 414–419. [CrossRef]
48. Tao, C.; Neutzner, S.; Collela, L.; Marras, S.; Kandada, A.R.S.; Gandini, M.; Bastiani, M.D.; Pace, G.; Liberato, M.; Caironi, M.; *et al*. 17.6% stabilized efficiency in low-temperature processed planar perovskite solar cells. *Energy Environ. Sci.* **2015**, *8*, 2365–2370. [CrossRef]